sustainability

MDPI

Article

Geothermal Characteristics and Productivity Potential of a Super-Thick Shallow Granite-Type Enhanced Geothermal System: A Case Study in Wendeng Geothermal Field, China

Haiyang Jiang [1,2,3,*], Liangliang Guo [4], Fengxin Kang [5,6,7], Fugang Wang [1,*], Yanling Cao [2,3], Zhe Sun [8] and Meng Shi [9]

[1] Key Laboratory of Groundwater Resources and Environment, Ministry of Education, Jilin University, Changchun 130012, China
[2] No.1 Institute of Geology and Mineral Resource Exploration of Shandong Province, Jinan 250010, China
[3] Shandong Engineering Laboratory for High-Grade Iron Ore Exploration and Exploitation, Jinan 250010, China
[4] College of Water Resources Science and Engineering, Taiyuan University of Technology, Taiyuan 030024, China
[5] 801 Institute of Hydrogeology and Engineering Geology, Shandong Provincial Bureau of Geology and Mineral Resources (SPBGM), Jinan 250014, China
[6] College of Earth Science and Engineering, Shandong University of Science and Technology, Qingdao 266590, China
[7] School of Water Conservancy and Environment, University of Jinan, Jinan 250022, China
[8] Tianjin Branch, CNOOC China Ltd., Tianjin 300459, China
[9] Shandong No.3 Exploration Institute of Geology and Mineral Resources, Yantai 264000, China
* Correspondence: hyjiang19@mails.jlu.edu.cn (H.J.); wangfugang@jlu.edu.cn (F.W.)

Abstract: Super-thick shallow granites without a cap layer are widely distributed in the Wendeng geothermal field. To evaluate the field's productivity potential for an enhanced geothermal system (EGS), we carried out field tests, laboratory tests and numerical simulations in succession. The geothermal characteristics and deep rock mechanical properties were identified based on real geological and core data from the borehole ZK1 in Wendeng geothermal field. Then, a numerical model of reservoir hydraulic fracturing based on a discrete fracture network was established. Thermal extraction simulations were then conducted to assess the long-term productivity of an EGS project based on the fracturing results. Possible well layout patterns and operational parameters were considered. Results indicated that, for naturally fractured formations, large well spacings should be used and reservoirs with overdeveloped natural fractures should not be selected. For the same reservoir, created by stimulation, the production performances of five-spot and triplet-well modes were different. The pressure indicator was more sensitive to the choice of well layout mode than the temperature indicator. The power generation of the five-spot well mode was slightly improved above that of the triplet-well mode. When selecting the target reservoir, the formations with high temperatures, moderate natural fractures, and high in-situ stress shielding are preferable. On this basis, a large volume of fracturing fluids should be injected to stimulate the reservoir, making the reservoir length and width as large as possible. If the desired large-scale reservoir is created, the five-point well mode should be selected.

Keywords: Hot Dry Rock; Enhanced Geothermal System; Hydraulic fracturing; well layout; heat production

Citation: Jiang, H.; Guo, L.; Kang, F.; Wang, F.; Cao, Y.; Sun, Z.; Shi, M. Geothermal Characteristics and Productivity Potential of a Super-Thick Shallow Granite-Type Enhanced Geothermal System: A Case Study in Wendeng Geothermal Field, China. *Sustainability* **2023**, *15*, 3551. https://doi.org/10.3390/su15043551

Academic Editor: Antonio Miguel Martínez-Graña

Received: 27 December 2022
Revised: 9 February 2023
Accepted: 13 February 2023
Published: 15 February 2023

1. Introduction

Geothermal energy is a clean and renewable energy source that can be developed for power generation and for direct use, such as space heating. Hot dry rock (HDR) resources denote high-temperature geothermal energy occurring in crystalline rock with low permeability and porosity. The total HDR resources within a 10 km depth all over

the world amounts to about 40–400 M EJ (1EJ = 10^{18}J), approximately 100–1000 times the quantity of fossil fuel energy [1]. In the past five years, the government of China has been actively investing in the exploration of HDR resources. Many potential HDR targets in China have been found, including the Songliao Basin, southern Hainan, Wendeng, Datong, Zhangzhou, Gonghe-Guide basin and Subei Basin [2]. In 2020, the government of China announced that China's carbon emissions will peak by 2030, and they will strive to achieve carbon neutrality by 2060. Large-scale non-carbon energy sources are urgently needed to improve China's energy structure. Therefore, HDR geothermal energy has attracted the attention of the government and researchers because of its huge reserves and low-carbon emissions.

Economical quantities of geothermal fluids cannot be obtained directly from HDR reservoirs due to their naturally low permeability. Enhanced geothermal systems (EGS), including reservoir stimulation and heat mining technology, can be adopted to extract the thermal energy stored in the HDR. Since the 1970s, numerous EGS projects have experimented with enhancing permeability at both existing and new geothermal sites. Pollack et al. reviewed and described challenges experienced in EGS projects, based on observations from 64 EGS sites [3]. Six sites ceased operations due to seismicity concerns. Drilling and plant operation issues, such as stuck drill strings and well collapses, delayed or terminated at least 24 EGS projects. At least 18 sites faced challenges in reservoir creation and circulation. The inability to raise financing either initially or in later project phases has been a major block for many EGS projects. While EGS sites have often encountered difficulties, at least 29 of the projects, including in-field and green field projects, continue to operate and generate electricity at an increasing rate.

Lessons learned from these EGS projects show that there are many factors affecting the final heat production of an EGS reservoir during the whole operational process. The stress state and rock properties of the target reservoir have an important influence on the geometry and permeability of the created reservoir [4]. When selecting the target reservoir for an EGS, the ideal target formation is one with a high temperature and well-developed natural fractures. The temperature factor is easy to determine, just by the selection of a high-temperature layer. However, better natural fracture development does not necessarily mean better productivity. This depends on fracturing and heat transfer effects. The effect of reservoir stimulation determines the amount of thermal energy that can then be extracted. During the heat-extraction stage, the well layout pattern and operational parameters affect the final productivity significantly. Therefore, the influence of reservoir characteristics and the stimulation scheme on heat-production performance from EGS should be investigated to optimize the heat-mining strategy.

Hydraulic shear stimulation in naturally fractured formation has been proven to be effective for power generation and has been used widely in EGS projects [5–7]. The fracture network is formed through the self-support of staggered natural fractures after fracturing [8,9]. For the stimulated EGS reservoir, there are mainly two methods for characterizing the fracture network for evaluating the heat-production performance: the equivalent continuous porous medium and real discrete fracture network [10,11]. The equivalent continuous porous method approximates the discrete fracture system as continuous porous media. Variants of this approach are the equivalent porous media method (EPM), the effective continuum method (ECM), the double-porosity method (DPM), and the multiple interacting continua (MINC) method. EPM is mainly used to model densely fractured reservoirs, where fracture density is high and fracture spacing is small, with the average fracture spacing less than 2~3 m, for example [5,10]. When the average fracture spacing is small, the EPM can attain good simulation results, while for large average fracture spacings, the DPM method gives better results [12]. The MINC method yields intermediate behaviors between a porous medium model and a single fracture model [13]. Suzuki et al. [14] conducted fractional diffusion modeling of heat transfer in porous and fractured media. They concluded that the porous media model matched the results of the MINC model for smaller fracture spacing (<5 m), while the single-fracture model agreed with the results of

the MINC model for larger fracture spacing (>20 m). Fracture networks are the dominant channels for water to transfer mass and heat in an HDR reservoir. A detailed description of the fractures is critical for numerical simulations. The discrete fracture network (DFN) model can be used to analyze the fracture orientation, size, spacing and other mechanical properties [15]. If the data of reservoir fracture distribution are adequate, the DFN model can be adopted.

Geological conditions and the fracturing scheme have a significant influence on fractured HDR reservoirs. Hence, the heat-extraction scheme should be optimized based on the results of the reservoir stimulation. Whether a formation is suitable as an EGS target reservoir is mainly determined by the final productivity performance. During the water circulation stage, the well pattern and operational parameters have important effects on thermal energy production. The main indices for evaluating EGS performance include power generation and flow impedance (or injectivity). The water production rate [16], production temperature [17], injection pressure [18], pump power [8,19], and energy efficiency [18,20], are also considered by many researchers.

Wendeng geothermal field has been developed for its hydrothermal geothermal resources for many years. This indicates that there exist abundant thermal resources in the underground. Super-thick shallow granites are widely distributed in Wendeng geothermal field. They are largely exposed to the surface without a cap layer, and their thermal structure is different from sedimentary-type geothermal fields. In order to evaluate whether this area has the potential for the development of HDR geothermal resources, Shandong provincial government has carried out a geothermal geological survey, drilling and logging in the Wendeng geothermal field area. The project is still in the feasibility study stage. The next plan is to select the appropriate reservoir for reservoir stimulation. In this study, we carried out field tests, laboratory tests and numerical simulations in succession to evaluate its productivity potential as an EGS. The geothermal characteristics and deep rock mechanical properties were identified based on real geological and core data from the borehole ZK1 in Wendeng geothermal field. Then, a numerical model of reservoir hydraulic fracturing based on discrete fracture network was established. Thermal extraction simulations were conducted to assess the long-term productivity of an EGS project based on the fracturing results. These research conclusions could serve as a reference for the development of future HDR geothermal resources in the Wendeng geothermal field.

2. Site Characteristics

2.1. Geological Background

Wendeng geothermal field is located in the east of the Shandong Peninsula in China (Figure 1a). It borders the Yellow Sea to the south. Tectonically, the Shandong Peninsula is located in the northwest side of the subduction zone between the Eurasian plate and the Philippine plate and is close to the western Pacific back-arc basin [21]. During the Mesozoic Indosinian period, a series of NS-trending tensional faults and NE-trending, NW-trending and EW-trending torsional faults were formed due to the strong brittle tension of the crust. Large-scale granitic magma intruded up the fault and formed some shallow dikes (Figure 1b). Thus, Wendeng geothermal field has good geothermal conditions and many hot springs. Exposed Meso-cenozoic magmatic rocks are widely distributed in the Wendeng geothermal field, and the thickness of the granite layer is up to 10 km [22].

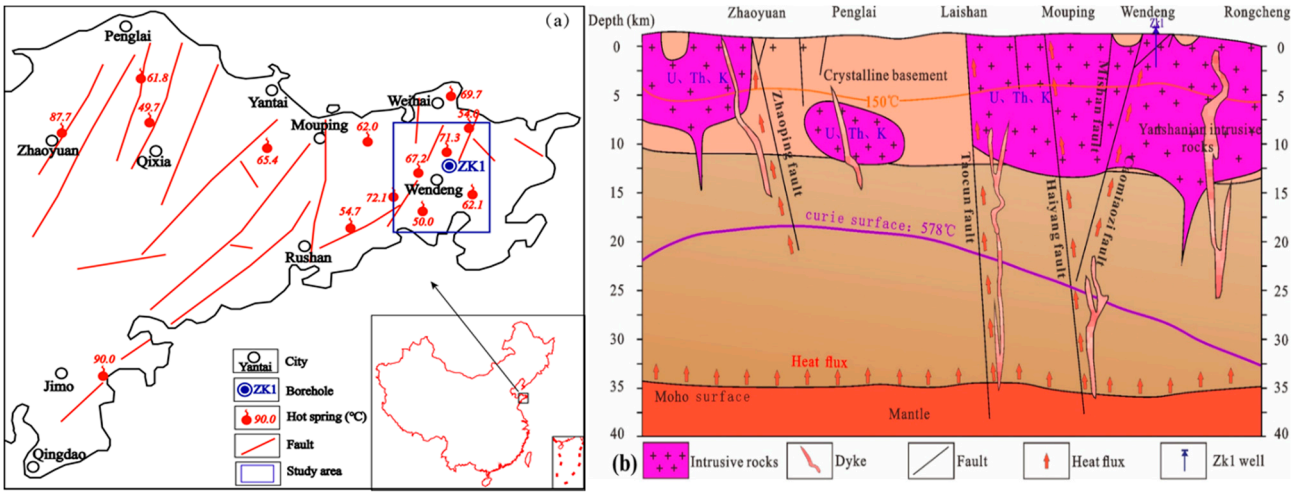

Figure 1. Location (**a**); and structure section map (**b**) of Shandong Peninsula [21,22].

2.2. Strata and Lithology

In 2018, the location of the deep geothermal borehole ZK1 was determined. It has a three-stage completion, with an opening diameter of 150 mm and a final diameter of 98 mm (Figure 2). In November 2019, the ZK1 well was completed to a depth of 3003.17 m. The core length is 2914.87 m in total. The lithology is mainly monzonitic granite, with high core integrity on the whole (Figure 2). A total of 20 diabase dykes were drilled, ranging in thickness from 2 m to 19.76 m, with different intrusion angles. Three hydrothermalized fractured zones were observed at 280 m~317 m, 625 m~660 m and 985 m~1015 m, respectively. These zones caused high fluid losses during drilling and had high geothermal gradients. The lithology at different depths has a similar geochemical composition, indicating that the strata were formed by the same magmatic intrusion.

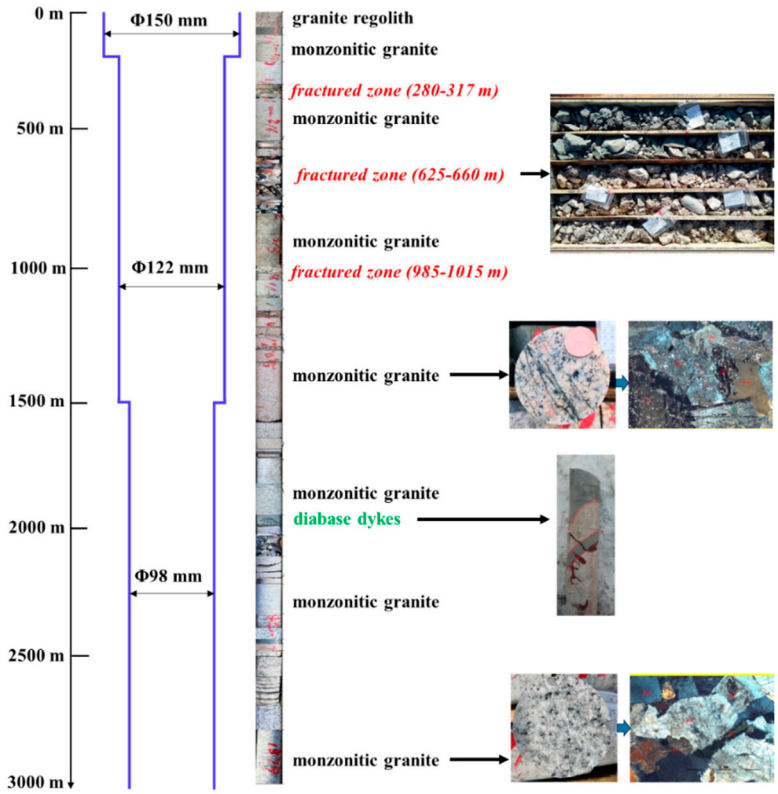

Figure 2. ZK1 borehole structure and formation lithology.

3. Methods

3.1. Field and Lab Test

The fracture ratio was obtained through comprehensive logging carried out on the whole borehole. In the measurement of field temperatures, the probe drop rate was set to about 6 m/min. The instrument recorded the temperature at intervals of 0.1 m. The sensitivity and accuracy of temperature measurement are ±0.01 °C and ±0.1 °C, respectively.

Rock samples were taken at intervals of 100 m (0~2000 m) and 50 m (2000 m~3000 m) to test their thermal-physical properties. Rock mechanics parameters were determined by tests on core samples from depths of 2950–3000 m.

3.2. Hydraulic Fracturing Simulation

The discrete fracture network (DFN) fracturing simulator MShale was used to model hydraulic fracturing in the target reservoir. MShale can simulate hydraulic fracture morphology in fractured and cave-dual media reservoirs [23]. The feasibility of using the DFN method of the MShale simulator for EGS fracturing has been proved by many scholars [6,24–26].

A series of laboratory tests were conducted to measure the mechanical and thermal parameters of core samples taken from the ZK1 well. The main rock mechanical parameters affecting hydraulic fracturing include the elastic modulus, Poisson's ratio, fracture toughness, and critical stress [27]. MTS 816.01 Direct shear test equipment was used to measure the mechanical parameters of core samples. The results showed that the elastic modulus is 70 GPa, Poisson's ratio is 0.16, fracture toughness is 1.5 MPa·$m^{1/2}$, and critical stress is 24 MPa.

Hydraulic shear fracturing in naturally fractured formations has been proven effective in EGS projects, thus it was adopted for simulation this time. For fracturing, the operational parameters include pump rate and injection fluid volume. The larger the pump rate, the greater the net pressure, and the more easily a complex fracture network is formed [28,29]. The maximum pump rate that can be achieved by domestic fracturing construction technology is about 16 m^3/min. The maximum injection volume was assumed to be 50,000 m^3.

The density of natural fractures has a great influence on fracturing results. The fracture network is formed through the self-support of staggered natural fractures after water shear fracturing. A formation with developed fractures is generally selected as the target reservoir. This study initially investigated the conditions when the natural fracture spacing was 20 m.

Longer fractures/fracture networks, more favorable for heat transfer, are formed when the reservoir is shielded by stress, which can increase the flow path from the injection well to the production well. In the vertical direction, the in situ stress usually varies with depth according to past EGS projects. Longer fractures would be formed when the reservoir is shielded by a high stress contrast at the upper boundary. Thus, the stress shielding layer is preferred when selecting the target reservoir. In summary, the following fracturing scenario (Case 1) was designed to represent a potential fractured reservoir (Table 1).

Table 1. Parameters of fracturing simulation under Case 1.

Parameters	Type	Values
Stress state	Shielding	Stress difference is 10 MPa Shielding thickness is 50 m
Mechanical parameters	Elastic modulus Poisson's ratio Fracture toughness Critical stress	70 GPa 0.16 1.5 MPa·$m^{1/2}$ 24 MPa
Operation parameters	Pump rate Injection volume	16 m^3/min 50,000 m^3
DFN	Fracture spacing	20 m

3.3. Thermal Extraction Simulation

3.3.1. Numerical Model, Parameters, Initial and Boundary Conditions

The TOUGH2-EOS1 code uses the integral finite difference method to solve the conservation equations of mass, momentum, and energy [30]. Their accuracy and reliability have been widely proven [2,4,6,8]. The MINC (Multiple Interacting Continua) approach is used to model flow in a fractured EGS reservoir. It is a generalization of the classical double-porosity concept developed by Warren and Root [31]. In the dual-porosity option, communication throughout the model is through the fractures, and communication between the fractures and matrix is through the inter-porosity flow defined by nested elements. Matrix blocks are discretized into a sequence of nested volume elements, which are defined on the basis of distance from the fractures [18,31].

The stimulated reservoir is discussed in Section 4.3. Because of symmetry, only half of the reservoir was included in the model. Figure 3 illustrates the 3D hydro-thermal numerical model of the stimulated reservoir. The geometric size of the model is 1000 m (x) × 700 m (y) × 200 m (z). The geometric size of EGS reservoir zone is 700 m (*x*) × 400 m (y) × 35 m (z) (Case 1 discussed in Section 4.3). To ensure that the simulation results are mesh-independent, the production temperatures after 20 years under various mesh numbers were obtained, as shown in Table 2. It can be observed that when the mesh number exceeds 7850, the production temperature remains nearly constant. Therefore, the simulations were conducted with a grid of 23 (x) ×32 (y) × 11 (z) and a total of 8096 primary cells. The matrix blocks were divided into four sub-grids with volume fractions of 0.08, 0.2, 0.35, and 0.35. The fracture domain occupied a volume fraction of 0.02. After this partition, there were a total of 40,480 sub-grid blocks nested in the 8096 primary grid blocks. In order to obtain reliable results, the grid was refined near the wells to accommodate the high pressure and temperature gradients.

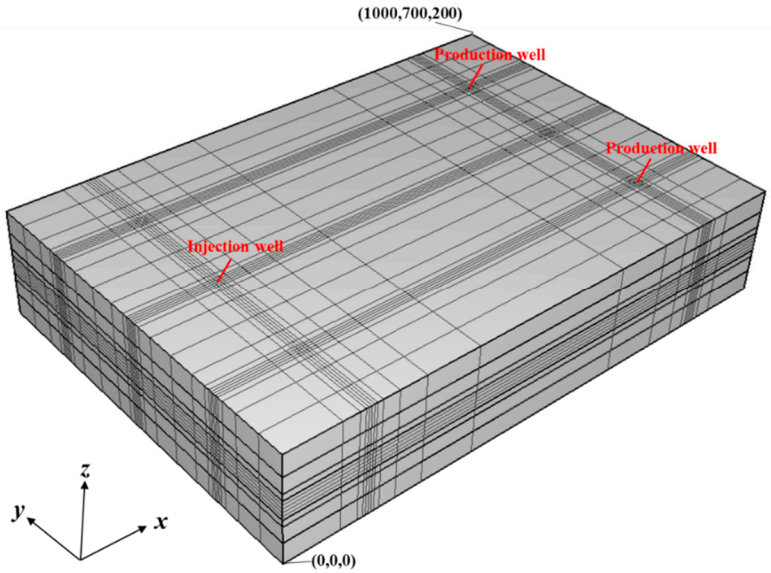

Figure 3. 3D schematic diagram of a numerical model of Case 1.

Table 2. Production temperature after 20 years under various mesh numbers.

Mesh Number	Production Temperature (°C)
3300	121.3
6600	120.4
7850	119.9
8420	119.8
9250	119.8

In this study, the boundaries of the EGS reservoir zone were open for mass and heat exchange with the surrounding rock. The model size was large enough to avoid the heat transfer impact from the boundary, and no flow and adiabatic condition were applied on the model boundaries. For simplification, the fracture was assumed to be unchanged during the simulation process. Water losses were ignored, and the injection rate was assumed to be equal to the production rate.

The EGS project was assumed to run for 20 years. The design injection temperature was 65 °C. When the temperature is lower than 65 °C, it can lead to scaling and chemical deposition, which would reduce the efficiency of heat extraction and cause damage to the EGS project [18]. Table 3 lists the reservoir parameters in the hydro-thermal simulation. The fracture permeability was calculated according to the cubic law with an aperture of 0.5 mm. The values of thermal conductivity and specific heat capacity were obtained from measured data.

Table 3. Reservoir parameters in the hydro-thermal simulation.

Items	Value
Matrix density	2650 kg/m^3
Matrix porosity	2%
Matrix permeability	1×10^{-17} m^2
Fracture permeability	0.21×10^{-8} m^2
Fracture spacing	20 m
Heat conductivity	3.52 W/(m·K)
Specific heat	850 J/(kg·K)
Initial pore pressure	P = 4×10^7 – 10,000z (Pa)
Injection water temperature	65 °C
Injection water specific enthalpy	305.80 kJ/kg
Initial reservoir temperature	181 °C
Productivity index	5.4×10^{-12} m^3
Production bottom-hole pressure	35 MPa

3.3.2. Production Performance Indicators

Production temperature (T_{pro}): the selection of different organic fluids in an organic Rankine cycle system results in specific requirements for production temperature [32]. Generally, the production temperature drop during the life of EGS project should be less than 10% [1].

Power generation (W_e): EGS has the highest priority for power generation, followed by heating. In this work, we presumed that all the extracted heat was used for power generation. The heat rejection temperature T_0 is 65 °C. If the utilization efficiency of maximum available work transferred to power is 0.45, then the power generation W_e can be calculated as

$$W_e = 0.45 q_{pro}(h_{pro} - h_{inj})(1 - \frac{T_0}{T_{pro}}) \quad (1)$$

where q_{pro} is the production flow rate; h_{pro} and h_{inj} are the bottom-hole production and injection specific enthalpy, respectively.

Bottom-hole injection pressure (P_{inj}): excessive injection pressure can cause closed fractures to reopen, leading to secondary reservoir growth. This growth is hard to define as either good or bad. However, excessive injection pressure requires greater pressure resistance from casing and surface lines, and it consumes more power. Therefore, the injection pressure should be as small as possible.

Flow impedance (I_R): this represents the power consumption of the unit production rate for penetrating the fractured reservoir. Water loss in the operation is ignored at this time. The injection flow rate is equal to the production flow rate. According to the experience with past EGS projects, I_R should be less than 0.1 MPa/(kg/s) as far as possible [1]. I_R is calculated by

$$I_R = (P_{inj} - P_{pro})/q \quad (2)$$

where P_{pro} is the bottom-hole pressure of the production well.

Energy consumption (W_p): It mainly includes the energy consumed by the injection pumps and the production pumps, which can be calculated using

$$W_P = \frac{q(P_{inj} - P_{pro}) - \rho q g(h_1 - h_2)}{\rho \eta_p} \quad (3)$$

where h_1 is the depth of the injection well and h_2 is the depth of production well. The average density ρ = 945 kg/m^3 is adopted for calculations. If the energy loss due to duct friction and water internal friction is neglected, the pump efficiency η_p is 80% [8].

Energy efficiency (η_e): the energy efficiency of EGS is the ratio of the total power generation to the internal energy consumption in the system. η_e can be calculated as Equation as

$$\eta_e = \frac{W_e}{W_p} = \frac{0.45\rho\eta_p(h_{pro} - h_{inj})(1 - T_0/T_{pro})}{(P_{inj} - P_{pro}) - \rho g(h_1 - h_2)} \quad (4)$$

4. Results

4.1. Geothermal Features

The trend line of temperature changes with depth was obtained (Figure 4). The average geothermal gradient was 36.8 °C/km between 0 m and 3000 m. The geothermal gradient decreased gradually from 55 °C/km at 200 m to 0 °C/km at 3000 m. Between 0 m and 1100 m, the formation temperature changes were almost linear. The reason is that the lithology is uniform, its thermal conductivity changes little, and there is no cap layer. Below 1100 m, the temperature drops because the well has penetrated along the water-conducting fault, which indicates a possible convection-type geothermal system. This is good for traditional hydrothermal geothermal development, but the temperature is still too low for a HDR reservoir, which require further drilling. Generally, geothermal gradients increase linearly with depth in this super-thick shallow granite area, as long as water-filled faults are not drilled. Therefore, when choosing shallow high-temperature HDR reservoirs in such super-thick granite areas, attention should be paid to avoiding deep fault zones.

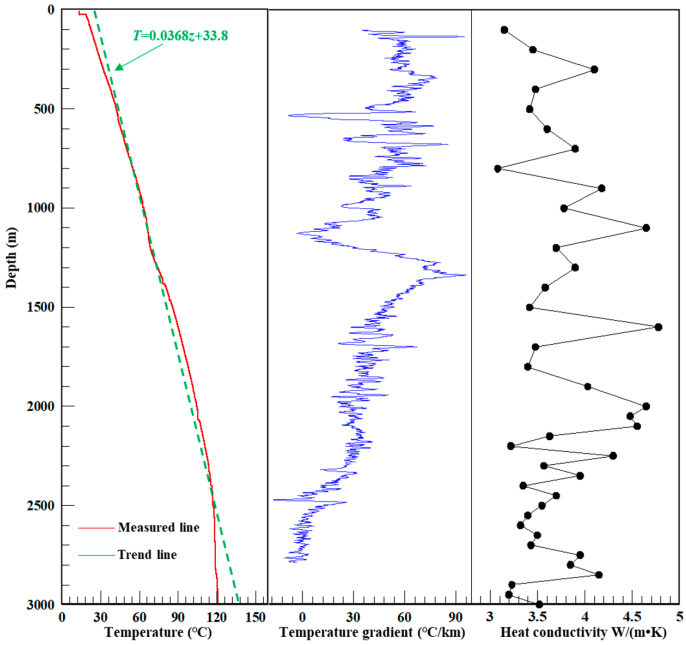

Figure 4. Results of temperature measurement and heat conductivity of ZK1 well.

The thermal properties of 40 core samples taken at different depths were obtained. Their heat conductivity ranged from 3.02 to 4.82 W/(m·K), with an average value of 3.52 W/(m·K). The average specific heat capacity was 850 J/(kg·K).

At present, the ZK1 well is only drilled to 3000.17 m, and the bottom-hole temperature is about 121.09 °C, which still corresponds to a middle-low temperature geothermal resource. To extract higher quality energy from the HDR resource, the well needs to be drilled deeper in the future. In this study, the formation at depth of 4000 m was initially selected as the potential target reservoir for production analysis. The formation temperature is expected to be about 181 °C at 4000 m if the deep formation belongs to conductive type of geothermal system.

4.2. Stress State

The natural formation is in a triaxial stress state. The size and morphology of hydraulic fractures are greatly affected by the in situ stress. During the process of drilling, the ZK1 well encountered 20 "broken cake" rock layers. "Broken cake" is an indicator of a high level of existing in situ stress. The thinner the cake, the higher the stress. Table 4 lists a total of five layers with a thickness of "broken cake" layer greater than 7 m. After drilling, the original stress condition is destroyed, leading to the cracking.

Table 4. Five main "broken cake" layers.

No.	"Broken Cake" Location	Thickness (m)	Pictures
1	2109.54 m~2264.17 m	244.63	
2	2342.74 m~2386.90 m	44.16	
3	2501.44 m~2551.19 m	49.75	
4	2615.06 m~2622.29 m	7.23	
5	2838.98 m~2872.51 m	33.53	

Hou proposed that once the in situ stress is large enough, "broken cake" core will occur [33]. The maximum horizontal principal stress (σ_H) can be deduced from the "broken cake" core characteristics according to the following equations

$$t < 0.35D \tag{5}$$

$$\sigma_H = \frac{\pi D \tau_0}{2t[4 - \frac{3t}{0.35D} + 0.5(\frac{t}{0.35D})^2]} \tag{6}$$

where t is the thickness of each "broken cake" core (mm); D is the diameter (mm); τ_0 is the shear strength.

In well ZK1, the thickness of "broken cake" core varies with depths. Taking the layer 2838.98~2872.51 m as an example, the thickness of "broken cake" core is mostly between 12 mm and 18 mm. The known core diameter is 62 mm, and the average shear strength is 24 MPa. Therefore, the calculated value of σ_H between 2838.98 m and 2872.51 m is 70.0~78.1 MPa.

After analyzing the hydraulic fracturing data from 13 oil wells in Shengli Oilfield in Shandong province [34], the stress magnitude as function of depth (for 1300 m~3300 m depth) can be summarized as

$$\sigma_H = -66 + 0.029H \quad (7)$$

$$\sigma_h = -124 + 0.023H \quad (8)$$

where H is the depth (m); σ_H is the maximum principal stress (MPa); σ_h is the minimum principal stress (MPa). The vertical principal stress (σ_v) is often calculated by $\sigma_v = \rho g h$. Thus, at the depth of 2850 m, the calculated in-situ stress is σ_H = 76.1MPa, σ_h = 53.2MPa, σ_V = 74.1 MPa. It can be seen that the difference of σ_H calculated according to Equations (6) and (7) is very small. It shows that horizontal stress plays a dominant role in the study area. Therefore, at the depth of 4000 m, the calculated σ_H, σ_h and σ_V are expected to be 109.4 MPa, 79.6 MPa and 103.9 MPa, respectively.

4.3. Stimulated Reservoir and Well Pattern

Table 5 shows the results for the stimulated fracture network under Case 1. Due to the limitation of stress shielding and the large maximum horizontal principal stress, the reservoir fracture network mainly extends in the horizontal direction.

Table 5. Results for the stimulated fracture network under Case 1.

Results	Values
L_{hf}	822.4 m
W_{hf}	410.5 m
H_f	50.0 m
SRA	675.0×10^4 m^2
SRV	4600×10^4 m^3

Horizontal or deviated wells were used in this study. The fracturing well was used as the injection well. The production wells are not fractured and are drilled directly through the boundary of the EGS reservoir (Figure 5). Due to the low permeability of the boundary zone of the fractures, the internal zone of the fracture network was selected as the simulated EGS reservoir. Based on the fracturing result, the thermal extraction well layout mode was set up as seen in Figure 6. The size of the EGS reservoir is 1400 m (Length) × 400 m (Width) × 35 m (Height). A triplet well layout mode was considered. It should be noted that the MShale simulator processes fractures into an orthogonal distribution. Thus, the injection and production wells are placed on the main fracture profile to obtain the longest flow path, as shown in Figure 6b. However, the natural fracture distribution has the characteristics of spatial heterogeneity. Well placement is strongly influenced by the fracture map and has a great impact on the heat productivity [35]. When more detailed reservoir information is available in the future, the effect of fracture properties should be considered in determining the well placement pattern.

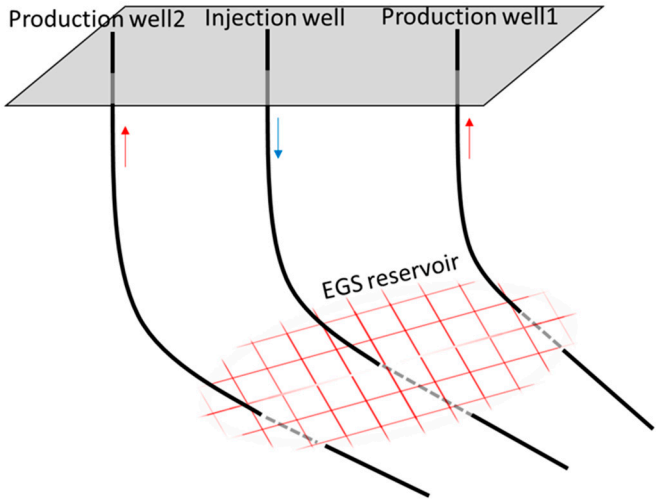

Figure 5. Schematic diagram of well layout.

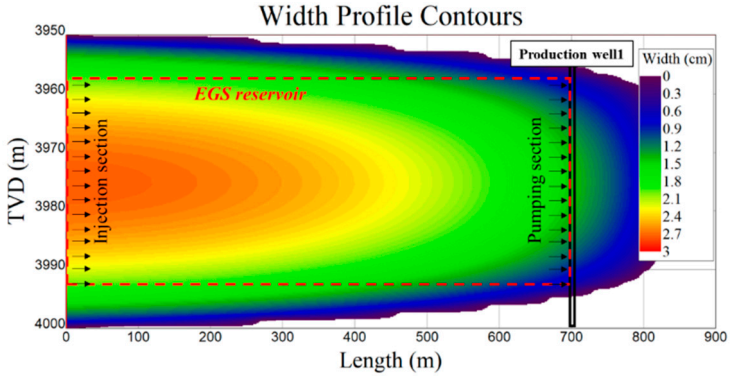

(**a**) Profile of main fracture. The red rectangle zone is the selected EGS reservoir area (side view).

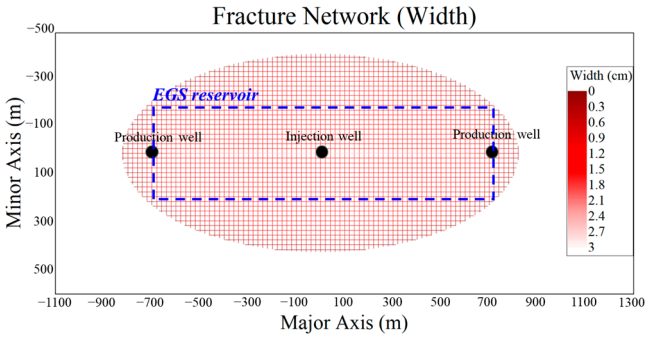

(**b**) Plan view: the blue rectangle zone is the selected EGS reservoir area (plan view).

Figure 6. Thermal extraction well layout mode under Case 1.

4.4. Heat Production Performance

Figure 7 shows the evolutions of T_{pro} and W_e at different injection rates (q_{inj}) over the 20 years. With the increase of injection rate, T_{pro} decreases continuously. When the injection rate is 20 kg/s, T_{pro} decreases down to 119.8 °C. When the injection rate increases to 70 kg/s, T_{pro} drops to 109.6 °C in the 5th year and 85.2 °C in the 20th year, which is 20.2 °C higher than the injection temperature. The higher the injection rate, the higher the W_e in the early stages of the project, but the decline rate of W_e is fast, and W_e is soon lower than that at the low injection rate. For 20 kg/s and 70 kg/s, for example, the two W_e curves

intersect in the fifth year. Five years later, the W_e at 20 kg/s is consistently higher than that at 70 kg/s.

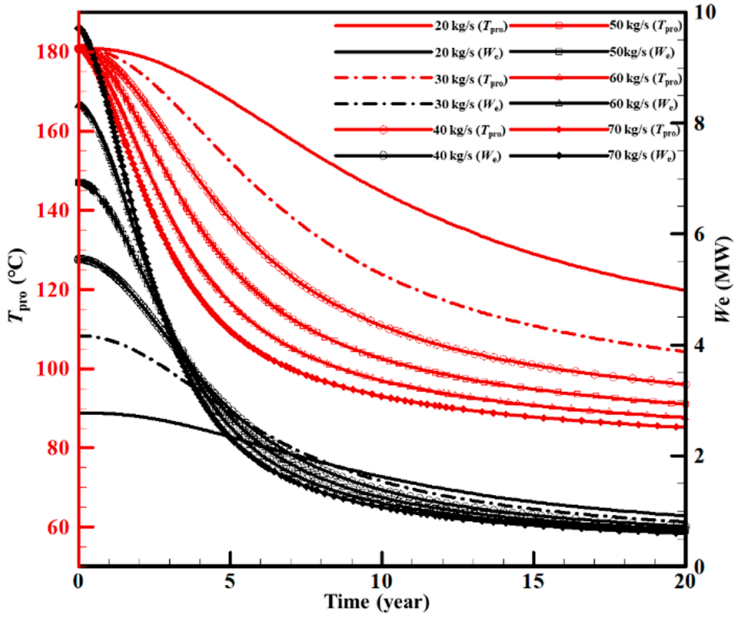

Figure 7. Evolution of T_{pro} and W_e at different injection rates (q_{inj}) over the 20 years under Case 1.

Figure 8 shows the evolutions of I_R and P_{inj} at different injection rates (q_{inj}) over the 20 years. The I_R and P_{inj} both increase with the increase of injection rate. During the 20 years of operation, the I_R and P_{inj} at 70 kg/s are, respectively, 0.03 MPa/(kg/s)~0.05 MPa/(kg/s) and 38.3 MPa~40.0 MPa.

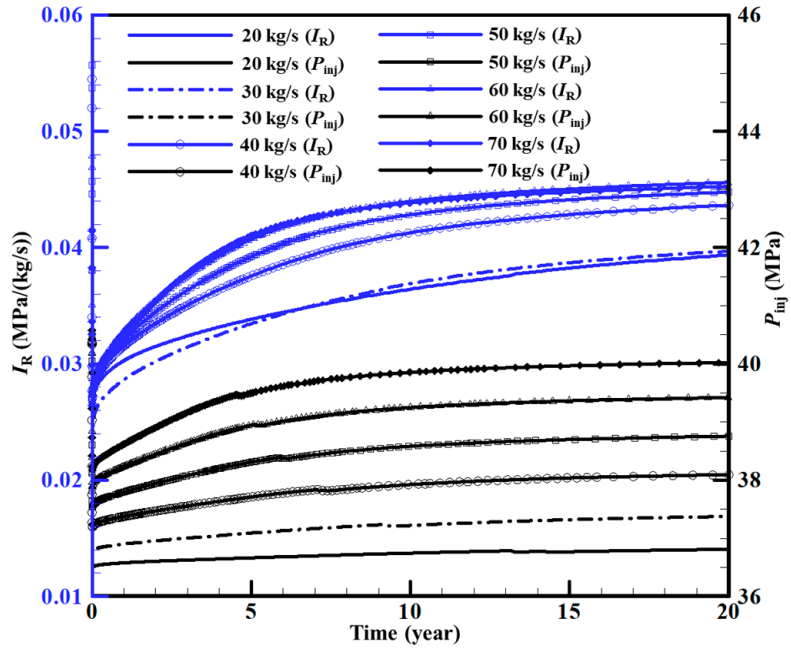

Figure 8. Evolutions of I_R and P_{inj} at different injection rates (q_{inj}) over the 20 years under case 1.

Figure 9 shows the evolution of W_P and η_e at different injection rates (q_{inj}) over the 20 years. As the injection rate increases, W_P increases, and its increment also increases. Since the W_e between different injection rates does not change much at the later stage of

the project, the efficiency η_e is greatly different. During the 20-year period, the efficiencies η_e at 20 kg/s and 70 kg/s are 197.2~44.1 and 57.2~2.1, respectively.

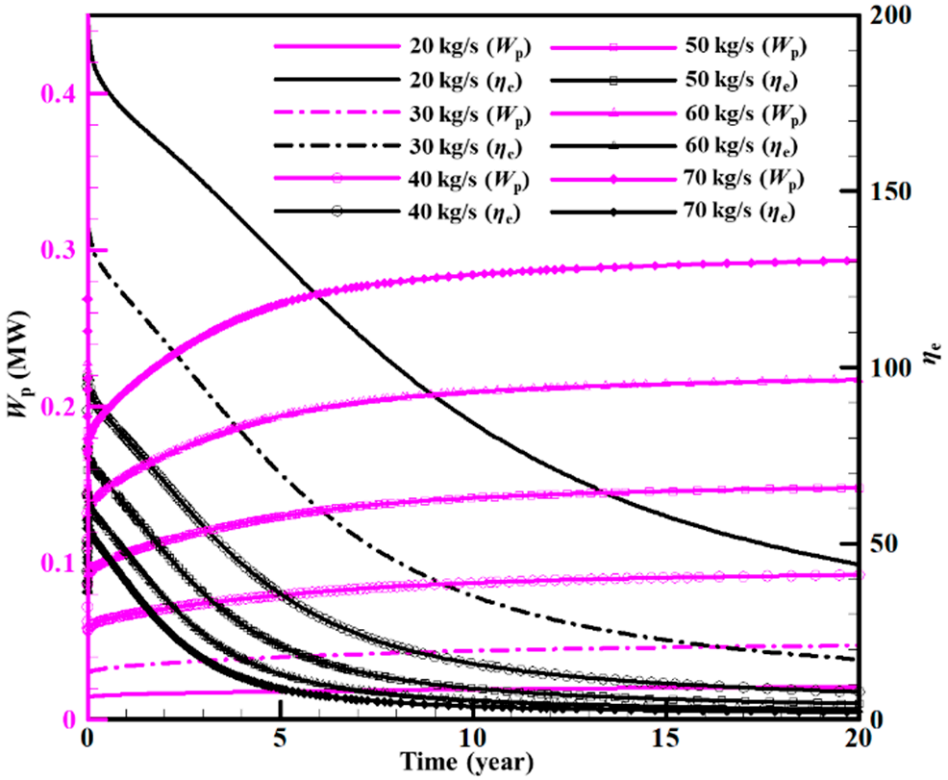

Figure 9. Evolution of W_P and η_e at different injection rates (q_{inj}) over the 20 years under Case 1.

For the stimulated reservoir, because its length and width are both large, the injected fluid has sufficient time to exchange heat with the reservoir. In addition, the fracture network reservoir has good connectivity between fractures, and so even when the injection rate reaches 70 kg/s, the I_R and P_{inj} indicators are still within the engineering allowable range. However, a too large injection rate results in large energy consumption and makes the energy efficiency decrease too fast. Thus, from the point of view of energy efficiency and power generation, an injection rate of 30 kg/s would be more suitable. For the triplet-well mode, the maximum injection rate is 60 kg/s, the power generation over 20-year period is 8.32 MW~1.62 MW, and the energy efficiency ranges from 142.4 to 17.1.

Figure 10 shows the spatial variations of reservoir temperature fields at the plane z = 100 m when q_{inj} is 30kg/s during the 20-year period. The cold halo expands fastest on the connection between the injection well and the production well (the axis). Due to better fracture permeability and connectivity, the cold halo has arrived at the production well by year 2.94. Then, the water flow mainly began to extract heat from the reservoirs on both sides of the axis. In the 20th year, the influence range of heat transfer at the side of the EGS reservoir has extended to 650 m at the plane z = 100 m.

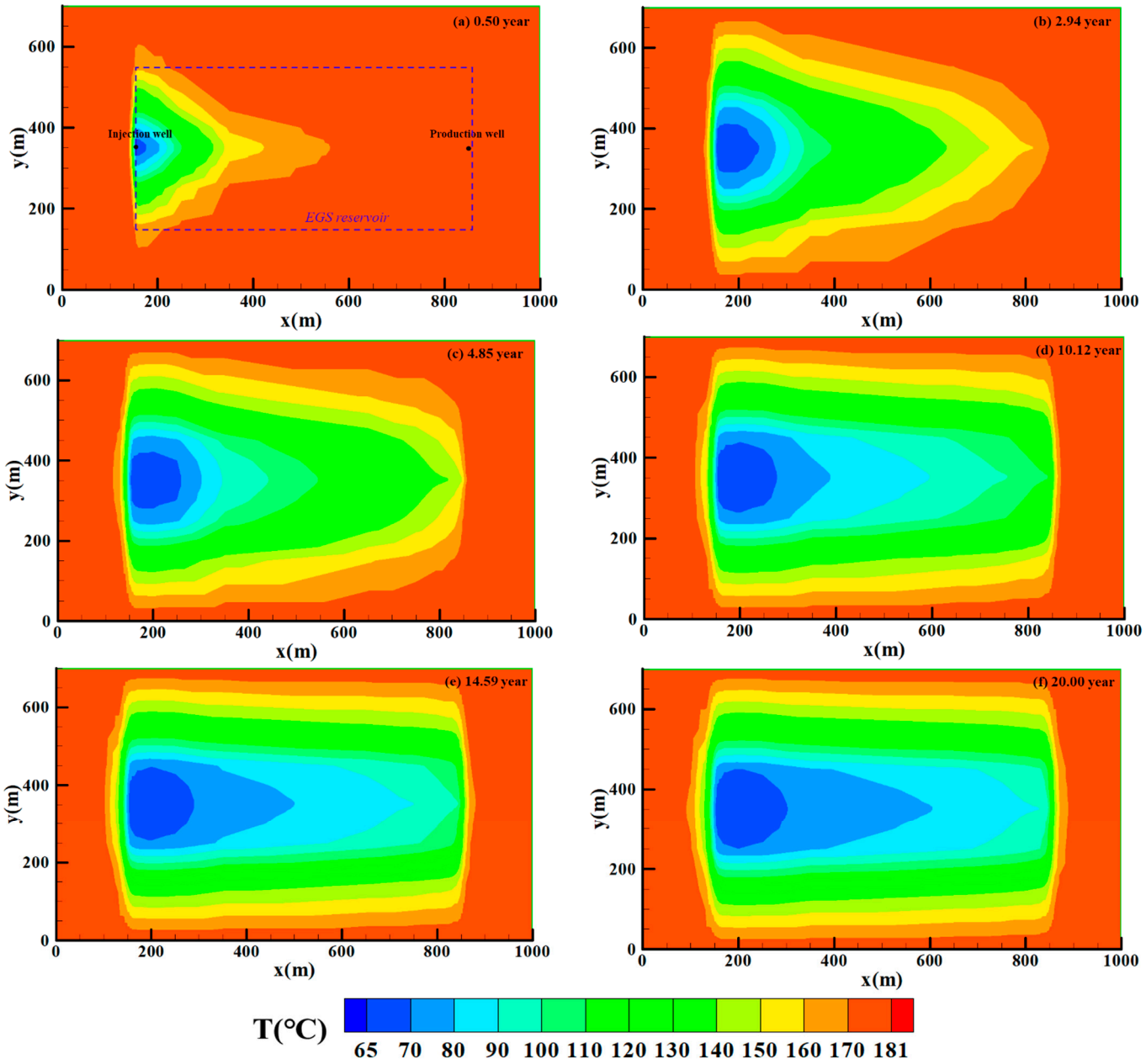

Figure 10. Spatial variations of reservoir temperature fields at the plane z = 100 m when q_{inj} is 30kg/s during 20 years (Case 1).

5. Discussions

5.1. Influence of Well Pattern on Production Performance

According to Section 4.3, the size of EGS reservoir under Case 1 is 1400 m (Length) × 400 m (Width) × 35 m (Height). Because the fracture network is long and wide, production wells can be drilled through different areas of the reservoir. Therefore, thermal extraction simulation analysis with a five-spot well layout mode (Case 2) was also considered to investigate the influence of the well-layout mode on heat-transfer performance (Figure 11).

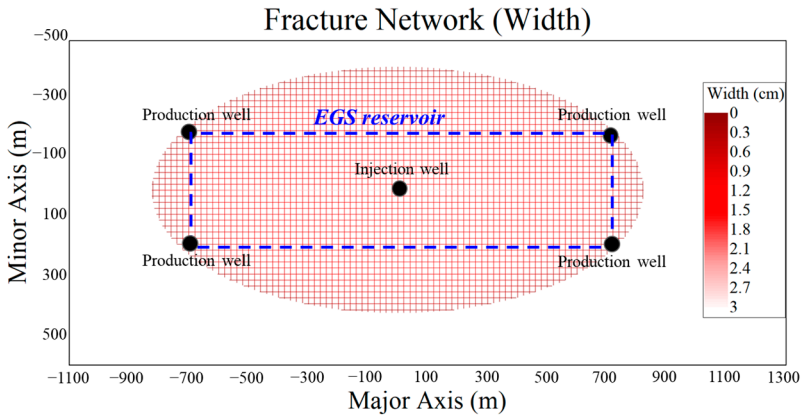

Figure 11. Thermal extraction with a five-spot well layout mode under Case 2.

Figure 12 shows the evolution of T_{pro} and W_e at different injection rates (q_{inj}) over the 20 years under Case 2. By comparing Figures 7 and 12, it can be seen that the variation trend of T_{pro} and W_e curves for Case 2 is almost the same as that for Case 1. However, at the same injection rate, the T_{pro} and W_e curves in Case 2 are both slightly higher than those in Case 1.

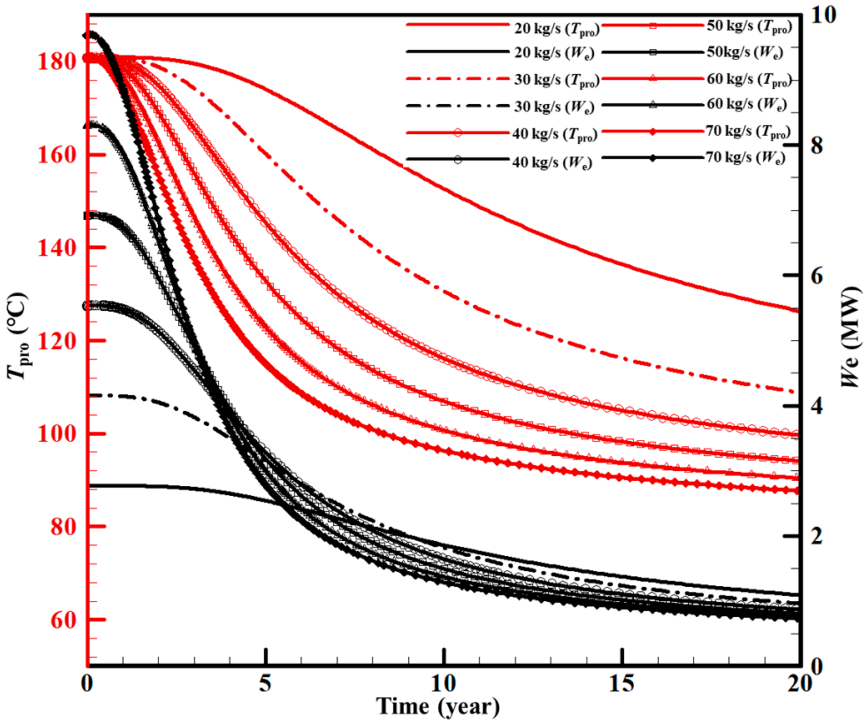

Figure 12. Evolution of T_{pro} and W_e at different injection rates (q_{inj}) over the 20 years under Case 2.

Figure 13 shows the evolution of I_R and P_{inj} at different injection rates (q_{inj}) over the 20 years under Case 2. The I_R and P_{inj} of Case 2 are both smaller than those in Case 1. For 70 kg/s, as an example, the I_R and P_{inj} are respectively 0.02 MPa/(kg/s)~0.03 MPa/(kg/s) and 37.0 MPa~38.2 MPa.

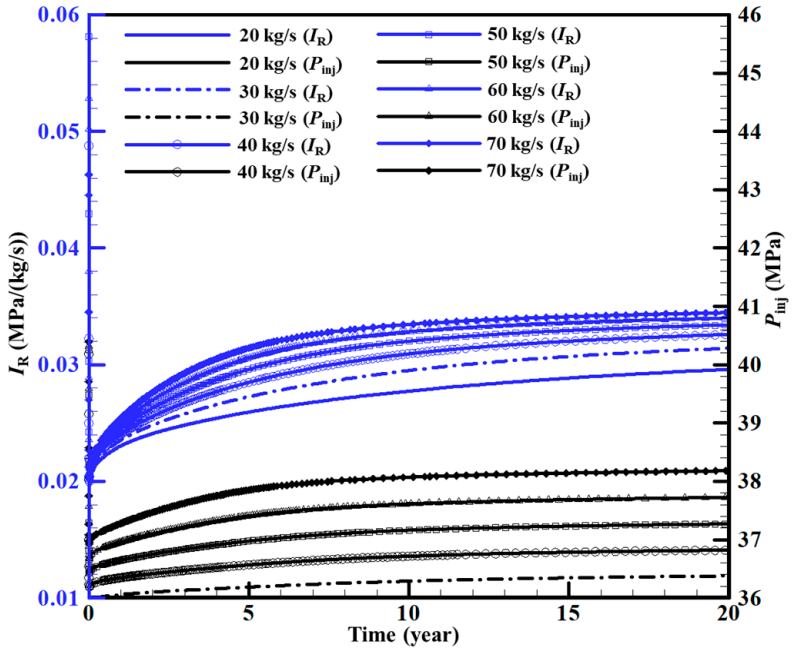

Figure 13. Evolution of I_R and P_{inj} at different injection rates (q_{inj}) over the 20 years under Case 2.

Figure 14 shows the evolution of W_P and η_e at different injection rates (q_{inj}) over the 20 years under Case 2. The W_P of Case 2 is smaller than that in Case 1, thus the η_e of Case 2 is higher than that in Case 1. The reason for the increasing pump consumption over time is that the temperature decreases, resulting in a viscosity increase, and this requires more injection pressure to push the fluid toward the production wells.

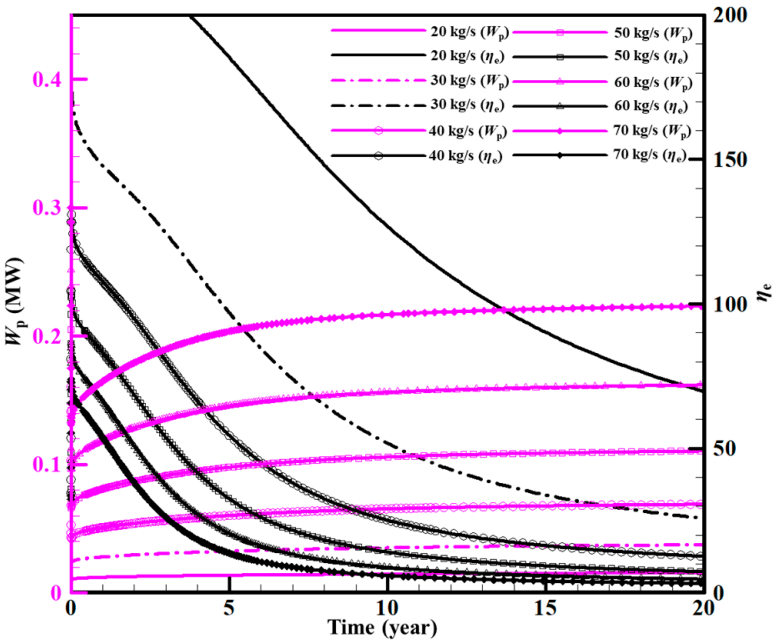

Figure 14. Evolution of W_P and η_e at different injection rates (q_{inj}) over the 20 years under Case 2.

Case 2 and Case 1 have the same reservoir, but different well-layout modes. Therefore, the variation trends of each indicator for the two cases are very similar, but the indicator values are different. The pressure indicator is more sensitive to the well-layout mode than the temperature indicator. For Case 2, from the point of view of energy efficiency and power generation, an injection rate of 30 kg/s or 40 kg/s would be more suitable. For

the five-spot well mode, and a maximum injection rate between 60 kg/s and 80 kg/s, the power generation over the 20-year period is 8.32 MW ~1.92 MW or 11.08 MW~1.74 MW, and the energy efficiency ranges from 176.5 to 25.8 or from 131.0 to 12.6. It can be seen that for the same reservoir, the production temperature of the five-spot well mode is slightly improved over that of the triplet-well mode (Figure 15). However, drilling extra-deep wells will increase the initial cost of the project.

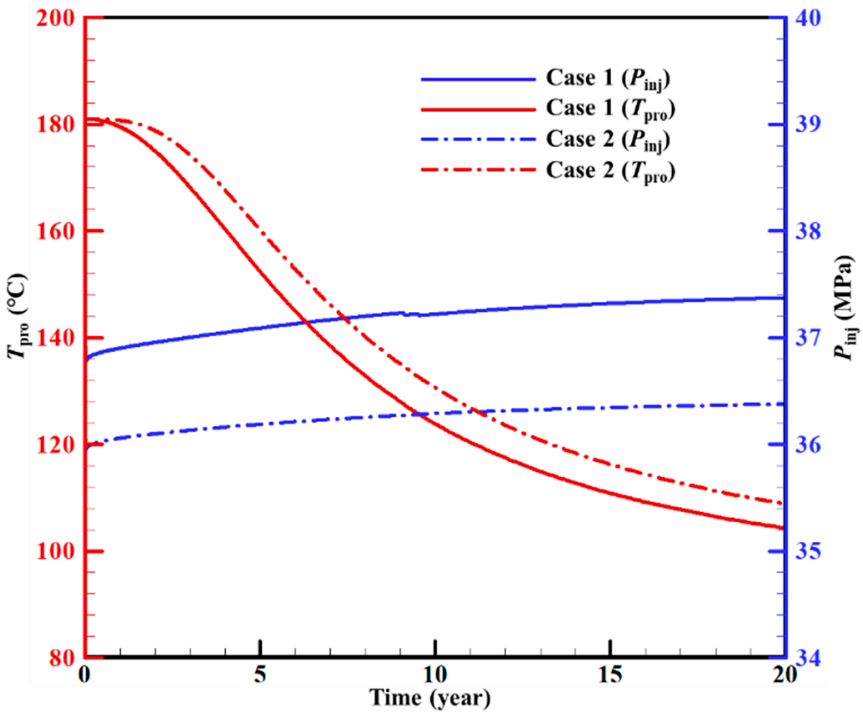

Figure 15. Comparison of T_{pro} and P_{inj} between Case 1 and Case 2 over the 20 years.

Figure 16 shows the spatial variations of reservoir temperature fields at the plan z = 100 m when q_{inj} is 30kg/s during 20 years under Case 2. Comparing Figure 10 (Case 1) and Figure 16 (Case 2), there are the following differences between them: (1) The temperature field on both sides of Case 2 are less affected by cold water injection than those of Case 1; (2) More heat was extracted from the EGS reservoir in Case 2 than from Case 1, with more cold zones in Case 2; (3) the area of low temperature in Case 2 is larger than that in Case 1 in the 20th year. Therefore, the five-spot well mode is better for energy extraction than the triplet-well mode for the same reservoir.

5.2. Influence of Fracture Spacing on Production Performance

The logging results for well ZK1 show that there are multiple fracture zones in the super-thick granite strata and the formation fracture ratio varies with depth (Figure 17). Generally, the formation with developed fractures is selected as the EGS reservoir. However, the fracture spacing may vary greatly at different depths. Therefore, the selection of the target EGS reservoir should consider the influence of fracture spacing.

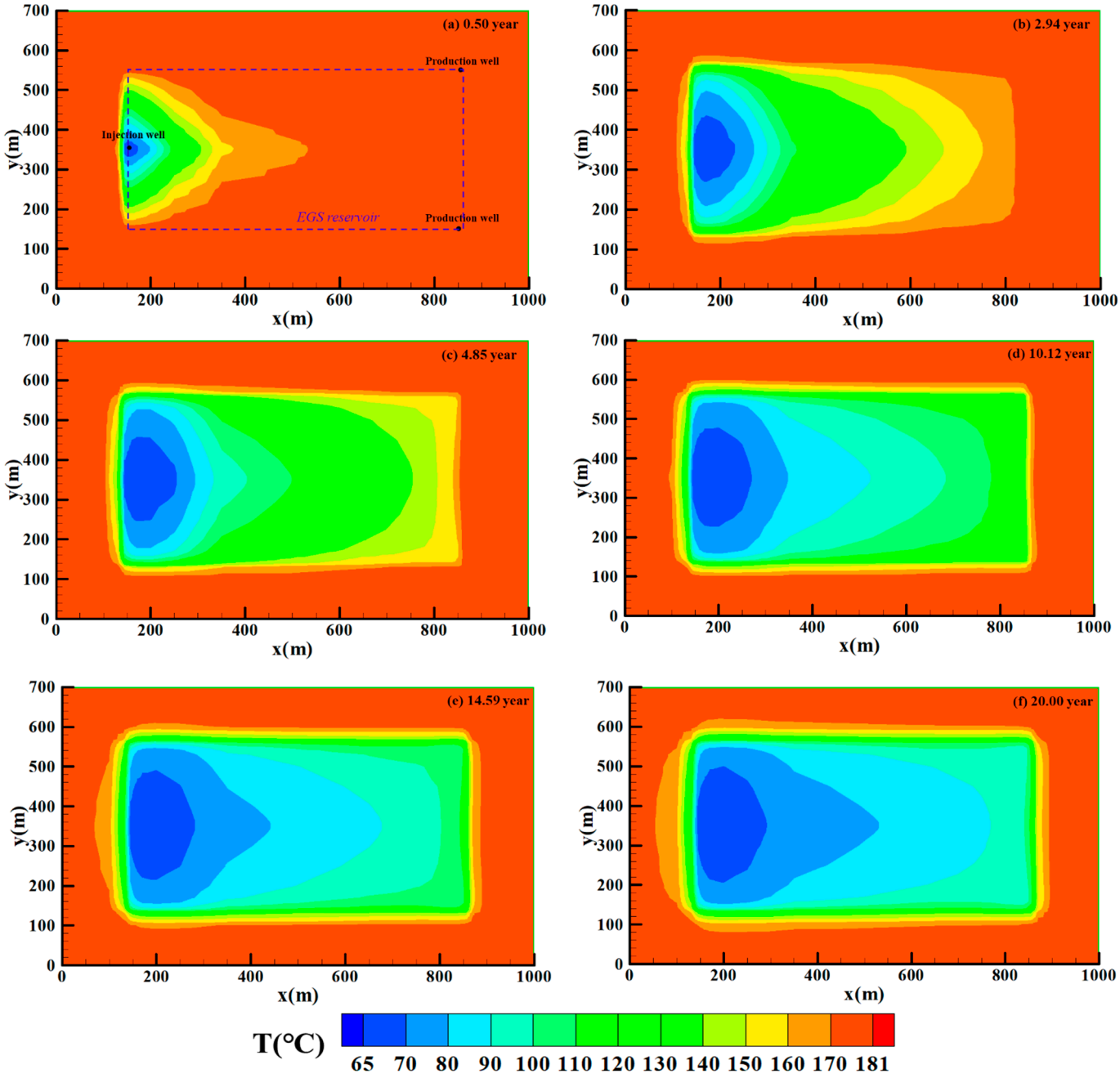

Figure 16. Spatial variations of reservoir temperature fields at the plane z = 100 m when q_{inj} is 30kg/s during 20 years (Case 2).

Figure 18 shows the characteristic parameters of stimulated fracture networks under different fracture spacing. With the increase of fracture spacing, the length, width and *SRV* of the fracture network all increase, while the *SRA* decreases. When the same fluid volume is injected, the larger the fracture spacing, the longer is the length of fracture network that is formed. Overall, the *SRV* is also larger. The decrease of the total fracture area indicates that the smaller the fracture spacing, the larger the heat exchange area is. When the fracture spacing increases from 0.5 m to 20 m, the half-length increases from 13.27 m to 75.61 m, an increase of 469.78%; the *SRV* increases by 3064.18% and the *SRA* decreases by 10.64%.

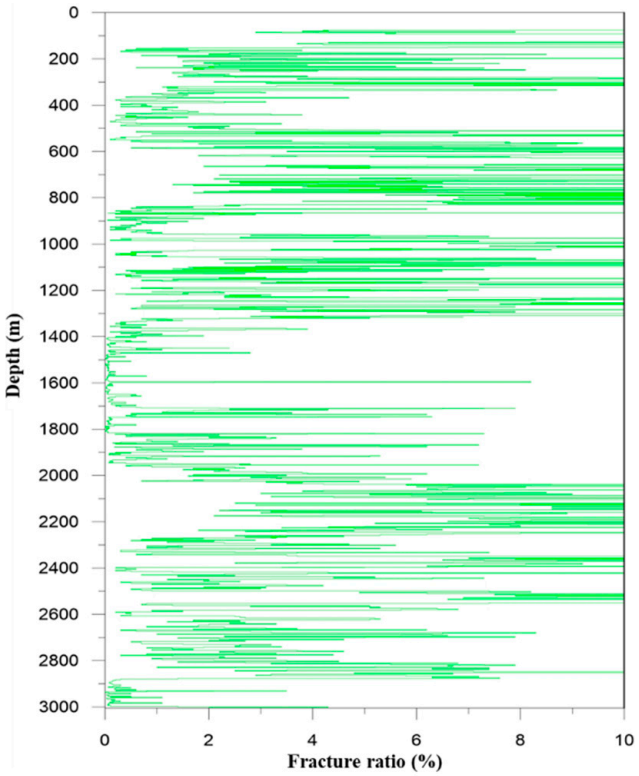

Figure 17. Formation fracture ratio at different depths of well ZK1.

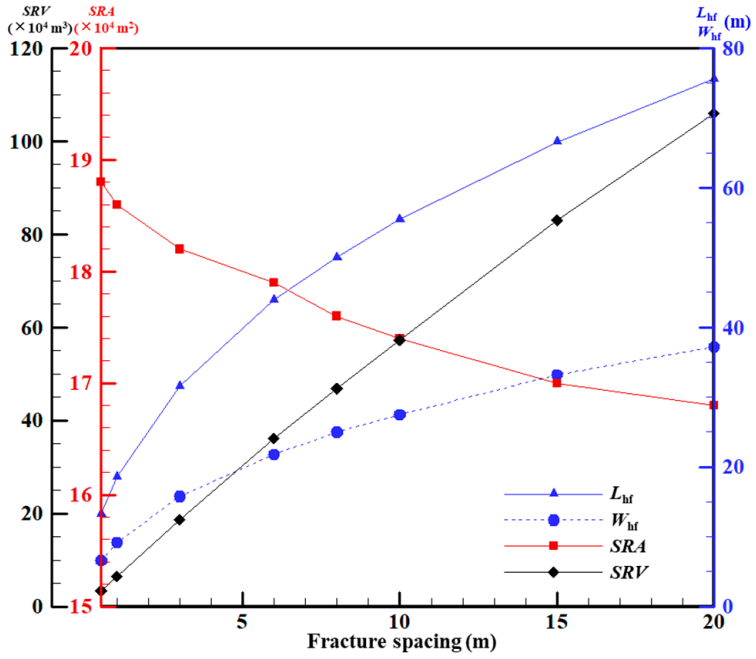

Figure 18. Characteristic parameters of the created fracture networks under different fracture spacing.

Based on the small fracture spacing of 0.5 m, representing a very developed fractured reservoir, fracturing simulation was performed to obtain the stimulated reservoir (Case 3). Table 6 lists the results of stimulated fracture network based on the natural fracture spacing of 0.5 m (Case 3). With the same volume of injection fluid, the reservoir size of Case 1 is much larger than that of Case 3. The Case 1 stimulation is more difficult to generate and more energy-consuming than Case 3 during actual fracturing operation. Then,

thermal extraction simulation analysis with triplet-well mode was carried out based on the fractured reservoir (Figure 19).

Table 6. Results of stimulated fracture network based on the natural fracture spacing of 0.5 m (Case 3).

Results	Values
L_{hf}	139.1 m
W_{hf}	68.3 m
H_f	50.0 m
SRA	700.0×10^4 m^2
SRV	123×10^4 m^3

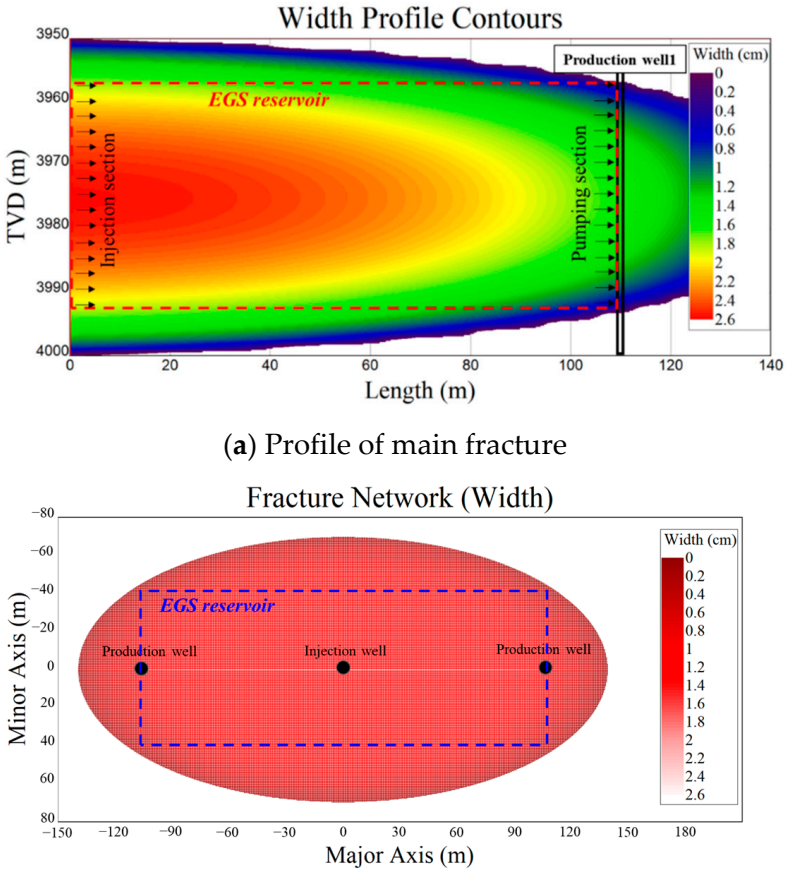

(**a**) Profile of main fracture

(**b**) Plan view

Figure 19. Thermal extraction with triplet-well layout mode under Case 3.

Figure 20 shows the evolution of T_{pro} and W_e at different injection rates (q_{inj}) over the 20 years under Case 3. The T_{pro} and W_e decrease with the increase of injection rate. At 1 kg/s, the T_{pro} is relatively stable at the beginning (0~1.5 a) and begins to decrease at the later stage. When the injection rate is greater than 3 kg/s, the T_{pro} drops rapidly at the initial stage of the project operation, and then enters a slow decline stage. The W_e also declines fast in the early stages.

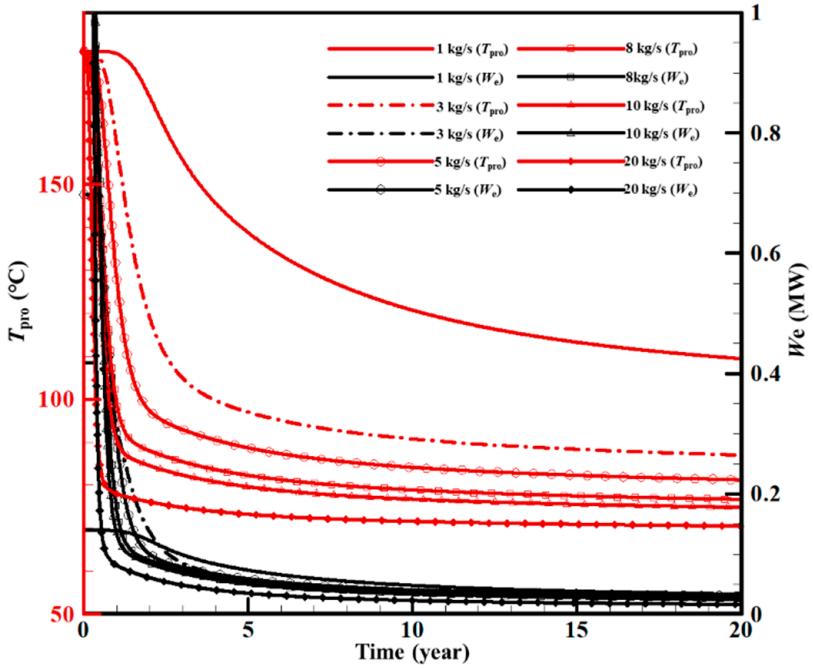

Figure 20. Evolution of T_{pro} and W_e at different injection rates (q_{inj}) over the 20 years under Case 3.

Figure 21 shows the evolution of I_R and P_{inj} at different injection rates (q_{inj}) over the 20 years under Case 3. The I_R and P_{inj} both increase rapidly in the early stages and then enter a slow rise stage. When the injection rate is 20 kg/s, the maximum I_R is 0.025 MPa/(kg/s) and does not exceed 0.1 MPa/(kg/s). The corresponding P_{inj} is 41.1 MPa, which increases by 1.1 MPa compared with the initial value.

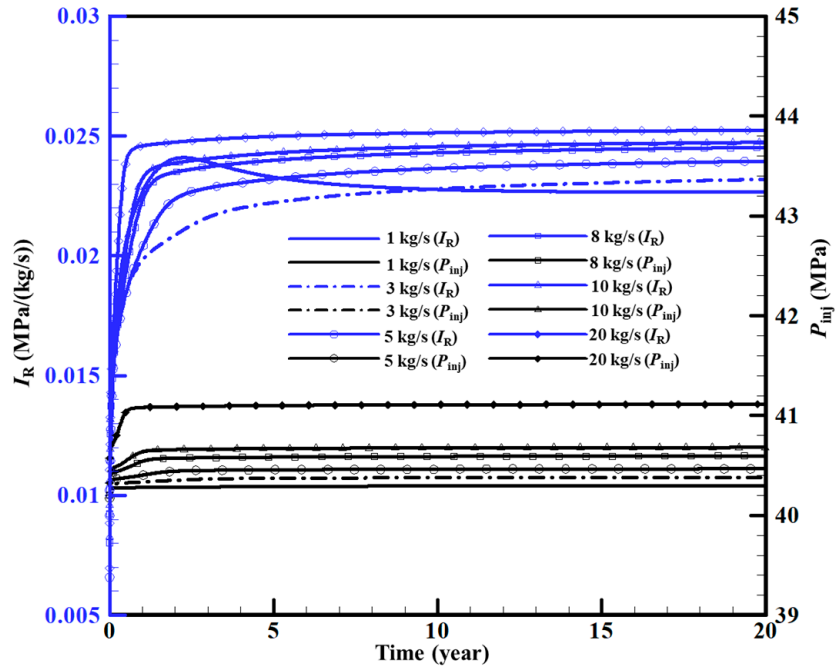

Figure 21. Evolution of I_R and P_{inj} at different injection rates (q_{inj}) over the 20 years under Case 3.

Figure 22 shows the evolution of W_P and η_e at different injection rates (q_{inj}) over the 20 years under Case 3. As can be seen, the W_P and η_e vary greatly with injection rate. At the injection rate of 1 kg/s, during the 20-year period the W_P is 1×10^{-5} MW~3×10^{-5} MW, and

the η_e is 10044~1118. Because the η_e of 1 kg/s and 2 kg/s are too large, these two cases are not reflected in the figure.

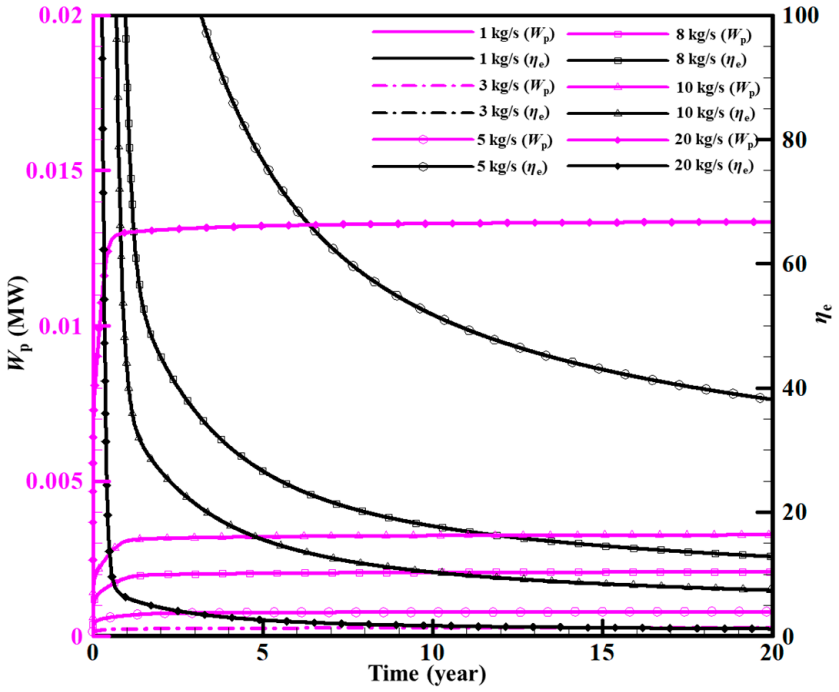

Figure 22. Evolution of W_P and η_e at different injection rates (q_{inj}) over the 20 years under Case 3.

Because the fractures in the EGS reservoir were very well developed (fracture spacing is 0.5 m) and the well spacing was only 110 m, a thermal short circuit occurred early, and the production temperature dropped very quickly. Meanwhile, the I_R and P_{inj} quickly reached a quasi-steady state after about two years. Thus, from the point of energy efficiency and power generation, an injection rate of 5 kg/s would be more suitable. For the triplet-well mode, the maximum injection rate is 10 kg/s, the power generations over the 20-year period are 1.40 MW~0.2 MW (0~2 a) and 0.2 MW~0.06 MW (2~20a), and the energy efficiency ranges from 2106.5 to 131.3 (0~2a) and from 131.3 to 38.1 (2~20a).

5.3. Recommendations for EGS Operation

Taking the above three cases together, Case 3 has a good reservoir stimulation effect, but due to the small well spacing and good permeability, the circulating water flow is short-circuited prematurely, and the final power generation is not ideal. For an EGS project with a doublet of wells to be profitable over a 25-year life cycle, the boreholes at depth should be at least 0.5–2 km from each other [1,3]. Longer reservoirs are preferred over thicker ones. Accurate measurement of the variation of in situ stress with depth is helpful for predicting the direction of the reservoir extension. At Rosemanowes, shallow stress measurements at 300m test wells did not correspond to stress measurements at the reservoir creation depth, which led to propagation of the stimulated zone in unexpected directions [1]. Thus, naturally fractured formations with stress shielding should be selected and well spacing should be maintained as large as possible. Meanwhile, reservoirs with overdeveloped natural fractures should not be selected in order to avoid premature thermal short circuit.

The most favorable option is Case 2, which has high injection rates and good power generation, but is prone to high pump costs when the reservoir length is too long, and the flow rate is too high. In addition, due to the lack of natural fractures (fracturing spacing is 20 m), it is difficult to stimulate such a large reservoir. It should be noted that the premise of the MINC method is good connectivity between fractures, even if the fractures are far apart. However, in practice, the size of self-supported fractures is too large to cause partial area closure, affecting the whole connectivity. Therefore, in theory, when selecting the target

reservoir, the formations with moderate natural fracturing, high in situ stress shielding and small shielding thickness are preferred. On this basis, a large volume of fracturing fluids should be injected to stimulate the reservoir, making the reservoir length as large as possible. The fracturing fluids can carry low concentrations of proppant to maintain fracture aperture and ensure overall connectivity of large fracture networks. If the desired large-scale reservoir is created, the five-point well mode is preferable.

6. Conclusions

In this paper, we carried out a field test, laboratory test and numerical simulation in succession to evaluate the EGS productivity potential of Wendeng geothermal field. The geothermal characteristics and deep rock mechanical properties were identified based on real geological and core data of the borehole ZK1. Then, a numerical model of reservoir hydraulic fracturing based on a discrete fracture network was established. Thermal extraction simulations were conducted to assess the long-term dynamic productivity of EGS based on the fracturing results. The main conclusions are shown as follows:

(1) For Wendeng geothermal field, the average geothermal gradient is 36.8 °C/km between 0 m and 3000 m. It can be seen that the temperature of the super-thick shallow granite reservoir in Wendeng geothermal field is not as high as the ideal, and the temperature change of shallow strata is almost linear. The reason is that the lithology is uniform and there is no insulating cap layer to keep in the heat. The high thermal conductivity of granite rocks radiates heat from below into the atmosphere. The deep geothermal gradient greatly decreases because it is controlled by tectonic faults and belongs to a convective geothermal zone. Therefore, when choosing shallow high-temperature HDR reservoirs in such super-thick granite areas, attention should be paid to avoiding deep water-filled faults.

(2) Wendeng geothermal field has high horizontal tectonic stress, which is conducive to forming a horizontal EGS reservoir after stimulation. The well-logging results show that there are also multiple fracture zones in the super-thick granite strata and the formation fracture ratio varies greatly at different depths. The selection of a target EGS reservoir should consider the influence of fracture spacing.

(3) For naturally fractured formations with stress shielding, large well spacings should be maintained and reservoirs with overdeveloped natural fractures should not be selected. For the same created reservoir, the production performance of five-spot and triplet-well modes of production is different. The variation trends of each production indicator of the two modes are very similar, but the indicator value is different. The pressure indicator is more sensitive to the choice of well-layout mode than the temperature indicator. For the same reservoir, the power generation of the five-spot well mode is slightly improved over that of the triplet-well mode.

(4) When selecting the target reservoir, formations with high temperatures, moderate natural fractures and high I -situ stress shielding are preferable. On this basis, a large volume of fracturing fluids should be injected to stimulate the reservoir, making the reservoir length as large as possible. If the desired large-scale reservoir is created, the five-point well mode is preferable.

(5) For the potential target reservoir at depth of 4000 m in the Wendeng geothermal field, the optimal scenario for an EGS reservoir is Case 2. With the five-spot well mode, and a maximum injection rate between 60 kg/s and 80 kg/s, the power generation over a 20-year period is 8.32 MW~1.92 MW or 11.08 MW~1.74 MW, and the energy efficiency ranged from 176.5 to 25.8 or from 131.0 to 12.6. It can be seen that the Wendeng geothermal field also has an HDR-resource development potential after reasonable screening of target reservoirs and good targeted fracturing and thermal extraction design.

As the stress regime of the study area is mainly a compressive one, it may close the fractures and reduce the hydraulic conductivity. In practical EGS projects, we suggest that one should be very careful when choosing which formation to use as the EGS target

reservoir. Additionally, a previous study showed that a large portion of the heat loss happens inside the wellbore and it may be more important than the reservoir response [36]. The wellbore model should be taken into account when a more accurate heat transfer simulation is carried out in the future. In this study, we used a simplified numerical model. Only the coupling of the hydraulic-thermal effect was considered and water losses in the reservoir were neglected. The distribution characteristics of the fracture spacing, aperture, and orientation should be collected to establish a more realistic hydraulic–thermal–mechanical–chemical model in the future.

Author Contributions: Conceptualization, H.J. and L.G.; methodology, L.G.; software, F.W. and Z.S.; validation, F.K. and M.S.; writing—original draft preparation, H.J.; writing—review and editing, L.G.; supervision, F.W. and Y.C. All authors have read and agreed to the published version of the manuscript.

Funding: This research was funded by Shandong Provincial Natural Science Foundation (ZR2020QD122, ZR2022QD060), No.1 Institute of Geology and Mineral resources of Shandong Province (2022DY09), Shanxi Basic Research Program Project (202203021211127), National Natural Science Foundation of China (grant numbers 42072331, U1906209).

Institutional Review Board Statement: Not applicable.

Informed Consent Statement: Not applicable.

Data Availability Statement: Some or all data, models generated or used during the study are available from the corresponding author by request.

Conflicts of Interest: The authors declare no conflict of interest.

References

1. Tester, J.W.; Livesay, B.; Anderson, B.J.; Moore, M.C.; Bathchelor, A.S.; Nichols, K.; Petty, S.; Toksöz, M.N.; Veatch, R.W. *The Future of Geothermal Energy: Impact of Enhanced Geothermal Systems (EGS) on the United States in the 21st Century*; An Assessment by an MIT-Led Interdisciplinary Panel; Massachusetts Institute of Technology: Cambridge, MA, USA, 2006.
2. Zhao, Y.; Shu, L.F.; Chen, S.Y.; Zhao, J.; Guo, L.L. Optimization Design of Multi-Factor Combination for Power Generation from an Enhanced Geothermal System by Sensitivity Analysis and Orthogonal Test at Qiabuqia Geothermal Area. *Sustainability* **2022**, *14*, 7001. [CrossRef]
3. Pollack, A.; Horne, R.; Mukerji, T. What are the challenges in developing enhanced geothermal systems (EGS)? Observations from 64 EGS sites. In Proceedings of the World Geothermal Congress, Reykjavik, Iceland, 1 April–1 October 2020; Volume 1.
4. Zhang, Y.; Zhang, Y.J.; Zhou, L.; Lei, Z.H.; Guo, L.L.; Zhou, J. Reservoir stimulation design and evaluation of heat exploitation of a two-horizontal-well enhanced geothermal system (EGS) in the Zhacang geothermal field, Northwest China. *Renew. Energy* **2022**, *183*, 330–350. [CrossRef]
5. Hofmann, H.; Babadagli, T.; Zimmermann, G. Hot water generation for oil sands processing from enhanced geothermal systems: Process simulation for different hydraulic fracturing scenarios. *Appl. Energy* **2014**, *113*, 524–547. [CrossRef]
6. Lei, Z.H.; Zhang, Y.J.; Hu, Z.J.; Li, L.Z.; Zhang, S.Q.; Fu, L.; Yue, G.F. Application of Water Fracturing in Geothermal Energy Mining: Insights from Experimental Investigations. *Energies* **2019**, *12*, 2138. [CrossRef]
7. Akdas, S.B.; Onur, M. Analytical solutions for predicting and optimizing geothermal energy extraction from an enhanced geothermal system with a multiple hydraulically fractured horizontal-well doublet. *Renew. Energy* **2022**, *181*, 567–580. [CrossRef]
8. Zeng, Y.C.; Su, Z.; Wu, N.Y. Numerical simulation of heat production potential from hot dry rock by water circulating through two horizontal wells at Desert Peak geothermal field. *Energy* **2013**, *10*, 92–107. [CrossRef]
9. Willis-Richards, J.; Wallroth, T. Approaches to the modeling of HDR reservoirs: A review. *Geothermics* **1995**, *24*, 307–332. [CrossRef]
10. Hayashi, K.; Willis-Richards, J.; Hopkirk, R.J.; Niibori, Y. Numerical models of HDR geothermal reservoirs- a review of current thinking and progress. *Geothermics* **1999**, *28*, 507–518. [CrossRef]
11. Wu, Y.S. The effective continuum method for modeling multiphase flow, multicomponent transport and heat transfer in fractured rock. In *Dynamics of Fluids in Fractured Rock*; Geophysical monograph 122; American Geophysical Union: Washington, DC, USA, 2000; pp. 299–312.
12. Gelet, R.; Loret, B.; Khalili, N. A thermal-hydro-mechanical coupled model in local thermal non-equilibrium for fractured HDR reservoir with double porosity. *J. Geophys. Res.* **2012**, *117*, 1–23. [CrossRef]
13. Mcdermott, C.I.; Randriamanjatosoa, A.R.; Tenzer, H.; Kolditz, O. Simulation of heat extraction from crystalline rocks: The influence of coupled processes on differential reservoir cooling. *Geothermics* **2006**, *35*, 321–344. [CrossRef]
14. Suzuki, A.; Fomin, S.A.; Chugunov, V.A.; Niibori, Y.; Hashida, T. Fractional diffusion modeling of heat transfer in porous and fractured media. *Int. J. Heat Mass Transf.* **2016**, *103*, 611–618. [CrossRef]

15. Patterson, J.R.; Cardiff, M.; Feigl, K.L. Optimizing geothermal production in fractured rock reservoirs under uncertainty. *Geothermics* **2020**, *88*, 101–906. [CrossRef]
16. Cheng, W.L.; Wang, C.L.; Nian, Y.L.; Han, B.B.; Liu, J. Analysis of influencing factors of heat extraction from enhanced geo-thermal systems considering water losses. *Energy* **2016**, *115*, 274–288. [CrossRef]
17. Shaik, A.R.; Rahman, S.S.; Tran, N.H.; Tran, T. Numerical simulation of Fluid-Rock coupling heat transfer in naturally fractured geothermal system. *Appl. Therm. Eng.* **2011**, *31*, 1600–1606. [CrossRef]
18. Yuan, Y.L.; Xu, T.F.; Jiang, Z.J.; Feng, B. Prospects of power generation from the deep fractured geothermal reservoir using a novel vertical well system in the Yangbajing geothermal field, China. *Energy Rep.* **2021**, *7*, 4733–4746. [CrossRef]
19. Yao, J.; Zhang, X.; Sun, Z.; Huang, Z.; Liu, J.; Li, Y.; Xin, Y.; Yan, X.; Liu, W. Numerical simulation of the heat extraction in 3D-EGS with thermal-hydraulic-mechanical coupling method based on discrete fractures model. *Geothermics* **2018**, *74*, 19–34. [CrossRef]
20. Yu, L.K.; Wu, X.T.; Hassan, N.S.; Wang, Y.D.; Ma, W.W.; Liu, G. Modified zipper fracturing in enhance d geothermal system reservoir and analyzed heat extraction optimization via orthogonal design. *Renew. Energy* **2020**, *161*, 373–385. [CrossRef]
21. Jiang, H.Y.; Wang, S.X.; Kang, F.X.; Shi, M.; Fan, Z.H.; Zhang, L. Geological characteristics and resource potential of dry-hot pore ZKCW01 in Wendeng, Shandong province. *Acta Geol. Sin.* **2019**, *93*, 217–225. (In Chinese)
22. Liu, C.H.; Sun, J.G.; Zheng, C.Q. Geochemical features and genesis of the Wendeng adamellitic rockbody, eastern Shandong province. *Jilin Geol.* **1995**, *14*, 51–58. (In Chinese)
23. Meyer & Associates. *Mayer Fracturing Simulators User's Guide*; Unicode Inc.: San Francisco, CA, USA, 2011.
24. Lei, Z.H.; Zhang, Y.J.; Zhang, S.Q.; Fu, L.; Hu, Z.J.; Yu, Z.W. Electricity generation from a three-horizontal-well enhanced geothermal system in the Qiabuqia geothermal field, China: Slickwater fracturing treatments for different reservoir scenarios. *Renew. Energy* **2020**, *145*, 65–83. [CrossRef]
25. Zeng, Q.D.; Yao, J. Numerical simulation of fracture network generation in naturally fractured reservoirs. *J. Nat. Gas Sci. Eng.* **2016**, *30*, 430–443. [CrossRef]
26. Hu, X.C.; Banks, J.; Guo, Y.T.; Liu, W.V. Utilizing geothermal energy from enhanced geothermal systems as a heat source for oil sands separation: A numerical evaluation. *Energy* **2022**, *238*, 121676. [CrossRef]
27. Zoback, M.D. *Reservoir Geomechanics*, 1st ed.; Cambridge University Press: Cambridge, UK; New York, NY, USA, 2007; p. 464.
28. Dezayes, C.; Genter, A.; Valley, B. Structure of the low permeable naturally fractured geothermal reservoir at Soultz. *Comptes Rendus Geosci.* **2010**, *342*, 517–530. [CrossRef]
29. Yoo, H.; Park, S.; Xie, L.; Kim, K.L.; Min, K.B.; Rutqvist, J.; Rinaldi, A.P. Hydro-mechanical modeling of the first and second hydraulic stimulations in a fractured geothermal reservoir in Pohang, South Korea. *Geothermics* **2021**, *89*, 101982. [CrossRef]
30. Pruess, K.; Oldenburg, C.; Moridis, G. *TOUGH2 User's Guide, Version 2.0*; Lawrence Berkeley National Laboratory: Berkeley, CA, USA, 1999.
31. Warren, J.E.; Root, P.J. The Behavior of Naturally Fractured Reservoirs. *Soc. Pet. Eng.* **1963**, *3*, 245–255. [CrossRef]
32. Garg, S.K.; Combs, J. A reformulation of USGS volumetric "heat in place" resource heat in place" resource estimation method. *Geothermics* **2015**, *55*, 150–158. [CrossRef]
33. Hou, F.L. Critical under-ground stress of disked rock cores and the relation between the thickness of rock disk and under-ground stress. *J. Wuhan Inst. Hydraul. Electr. Power* **1985**, *1*, 37–48. (In Chinese)
34. Ding, J.M.; Liang, G.P.; Guo, Q.L. Stress measurements in deep borehole along bohai coastal area in Shandong province-determination of the magnitude of principal stress. *J. Seismol.* (In Chinese). **1986**, *5*, 1–8.
35. Mahmoodpour, S.; Singh, M.; Bär, K.; Sass, I. Impact of Well Placement in the Fractured Geothermal Reservoirs Based on Available Discrete Fractured System. *Geosciences* **2022**, *12*, 19. [CrossRef]
36. Mahmoodpour, S.; Singh, M.; Turan, A.; Bär, K.; Sass, I. Hydro-Thermal Modeling for Geothermal Energy Extraction from Soultz-sous-Forêts, France. *Geosciences* **2021**, *11*, 464. [CrossRef]